J. Eur. Opt. Society-Rapid Publ. 2026, **22**, 23

https://doi.org/10.1051/jeos/2026016
Available online at: https://jeos.edpsciences.org

EOSAM 2025
Guest editors: Omar El Gawhary, Stefan Witte, Ignacio Moreno

Journal of the European Optical Society-Rapid Publications

Review Article OPEN ACCESS

Fano-like resonance in optical fiber

Vinicius Piaia, Paulo Robalinho, Susana Silva, and Orlando Frazão*

INESC TEC – Institute for Systems and Computer Engineering, Technology and Science, 4169-007 Porto, Portugal

Received 24 November 2025 / Accepted 18 February 2026

Abstract. Fano resonances emerge from the coherent interference between a discrete resonant state and a continuum of propagating modes, giving rise to a characteristically asymmetric spectral line shape with heightened sensitivity to minute variations in the underlying physical parameters. This study provides a chronological perspective on the development and increasing implementation of Fano-type effects in fiber-optic technology. Their implementation in fiber Bragg gratings (FBGs) through numerical simulations of resonant Fano behavior. Specifically, a Fano-like response in an FBG can be designed by introducing a tailored phase shift into the grating structure; the magnitude of this phase discontinuity constitutes an effective control parameter for tuning the interference condition and, consequently, the resulting spectral asymmetry. The resonance produces a distinctive, asymmetrical spectral response that is attractive for a broad range of photonic functionalities. Key applications include fiber-integrated sensing – where the enhanced spectral sensitivity supports the detection of changes in refractive index, temperature, pressure, or biomolecular interactions – as well as narrowband filtering and spectral shaping for telecommunications and optical signal-processing systems.

Keywords: Fano-like resonances, Optical fibers, Gratings structures and interferometry.

1 Introduction

In the literature, Fano resonances have been extensively reported across a wide range of photonic systems, underscoring their fundamental importance in controlling light–matter interactions and enabling novel optical functionalities. Representative examples include artificial photonic molecules [1], Fano lasers [2], metamaterials [3], nanophotonic structures [4], photonic crystals [5], semiconductor nanostructures [6], plasmonic nanoantennas [7], optical switches [8], all-optical modulators [9], dielectric metasurfaces [10], and topological photonic systems [11], among others. The ubiquity of Fano-type interference across such diverse platforms highlights both the universality and tunable nature of this phenomenon, which continues to attract significant interest for applications in optical filtering, switching, nonlinear photonics, and high-resolution sensing.

Despite these remarkable advances, many existing implementations rely on intricate geometries or complex fabrication techniques, which can restrict scalability and practical deployment. In this context, fiber-based platforms offer unique advantages, combining the inherent merits of optical fibers – such as low transmission loss, compact form factor, mechanical flexibility, and compatibility with existing telecommunication infrastructures – with the enhanced spectral sensitivity and selectivity enabled by Fano resonances.

This review traces the evolution of research on Fano resonance in fiber-optic systems, revealing a clear trajectory from the first fundamental demonstrations in the mid-2000s to the emergence of advanced, tunable, and application-driven devices after 2020. It then presents the main structures used to induce Fano resonance in optical fiber devices, such as whispering-gallery-mode resonators, microstructured optical fibers, interferometric devices, and FBGs. To exploit FBG applications, a theoretical model of a Fano-FBG is introduced, which captures the spectral evolution as either the FBG reflectivity or the fiber-end environment reflectivity is varied. Finally, the model is demonstrated in a self-referenced refractive-index sensor as one of the possible applications.

2 Fano concept

A deeper understanding of the wave-like behavior of light has enabled the development of advanced optical technologies. Among the most significant properties exploited in these innovations is resonance, which has played a central role in many of the scientific community's major achievements. Resonant cavities constitute the foundation of widely used optical devices, including lasers, Fabry–Pérot

* Corresponding author: orlando.frazao@inesctec.pt

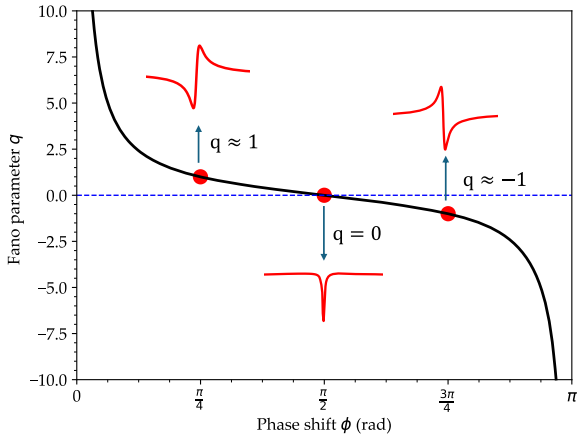

Fig. 1. Dependence of the Fano parameter q on the phase shift of the continuum mode, with the resulting line shapes: asymmetric for $q \approx \pm 1$ and quasi-Lorentzian for $q = 0$.

interferometers (FPI), and Bragg gratings. Fano resonance was first demonstrated by Ugo Fano in his investigation of inelastic electron scattering by helium [12], revealing an asymmetric line shape with a high-quality factor. It was established that this resonance arises when a discrete mode spectrum interferes with a continuous mode spectrum. This interaction is described by the spectrum $\sigma(E)$, as expressed in equation (1) [13].

$$\sigma(E) = 4\sin^2\phi \frac{(q+\Omega)^2}{1+\Omega^2}. \quad (1)$$

Here, $q = \cot\phi$ is the Fano parameter, with ϕ the continuum phase shift and E the spectral energy. The dimensionless variable $\Omega = 2(E - E_0)/\Gamma$ is defined by the resonance energy E_0 and linewidth Γ. Originally introduced for absorption spectra, the model also describes transmission, reflection, and scattering, highlighting its versatility in optical devices. The parameter q governs spectral asymmetry: for $q \approx \pm 1$, strong discrete–continuum coupling produces asymmetric line shapes, while for $|q| \gg 1$ or $q \approx 0$, weaker coupling yields Lorentzian-like profiles. In Figure 1 shows the dependence of the Fano parameter q on the phase shift.

3 Historical overview

Between 2005 and 2015, only a limited number of papers were published in this field, reflecting the exploratory nature of Fano resonance at the time and the early emergence of its application in fiber-based structures. Figure 2 presents a timeline of the annual number of articles on Fano resonance in fiber-optic systems published between 2005 and 2025.

Chiba et al. [14] reported that Fano resonances can be induced in a multimode tapered fiber waveguide coupled with a high-Q microspherical cavity, without requiring any additional elements such as reflectors or delay optics. Steinvurzel et al. [15] demonstrated that the scattering resonances of a single cylinder correspond to Fano resonances, which indeed appear in the loss spectra of solid-core photonic bandgap fibers (PBFs). Totsuka et al. [16] performed Fano resonance to yield coupled-resonator-induced transparency. Vincetti and Setti [17] reported that Fano resonances between hollow-core modes and higher-order dielectric modes occur within the transmission bands. Li et al. [18] observed Fano resonances in a single whispering-gallery microresonator. Furthermore, Vincetti and Setti [19] showed that the additional losses in Kagome fiber designs arise from Fano resonances between core modes and cladding modes exhibiting strong spatial dependence. Chang and Solgaard [20] presented Fano resonances in integrated silicon Bragg reflectors, highlighting their potential for sensing applications. Finally, Yu et al. [21] reported the control of Fano resonances in photonic crystal structures and demonstrated their application in ultrafast optical switching. Yang et al. [22] demonstrated an aerostatically tuned microbubble whispering-gallery resonators to obtain an electro-magnetic-induced transparency and Fano-like lineshapes to sensing application. Over the last decade, Figure 3 highlights a marked increase in the use of resonant waveguide structures in optical fibers, underscoring a strong potential that remains not yet fully explored in this field.

In 2016, Miao et al. [23] reported the evolution of Fano resonance in a thin fiber taper–coupled cylindrical microcavity. Unlike enclosed microcavities, the cylindrical configuration supported both localized whispering gallery modes (WGMs) and delocalized radiation modes. Zhao et al. [24] demonstrated a simple method to achieve Fano-like resonance by coupling a microsphere resonator with a fiber Mach–Zehnder interferometer (FMZI). In their configuration, a tapered microfiber was integrated into one arm of the interferometer to enable evanescent coupling with the microsphere resonator. Gu et al. [25] investigated a fiber loop laser stabilized by Fano resonance in a metallic grating–coupled resonator, demonstrating improved spectral stability. Liao et al. [26] developed a technique to reduce the spectral density of a microbottle resonator (MBR) by depositing UV-curable adhesive droplets near the resonator's central region, effectively degrading the Q-factors of high-order bottle modes and enhancing resonance selectivity.

In 2017, several studies expanded the understanding and applications of Fano resonance in optical systems. Lin et al. [27] proposed a novel microstructured optical fiber (MOF) for multichannel sensing based on Fano resonance among different WGMs propagating through the fiber. The proposed MOF comprised multiple capillary channels of varying diameters arranged within a tubular framework. Miao et al. [28] demonstrated a ring fiber laser structure based on a thin fiber taper–coupled microcylinder system functioning as a transmissive optical filter that selectively allowed narrowband modes to propagate. Li et al. [29] carried out theoretical and numerical investigations of three distinct types of Fano resonances, each arising from different physical mechanisms, in a plasmonic resonator composed of two circular cavities. Zhang et al. [30] proposed a cone-shaped inner-wall coupler to efficiently excite WGMs in a microsphere resonator, while Zhang et al. [31] reported

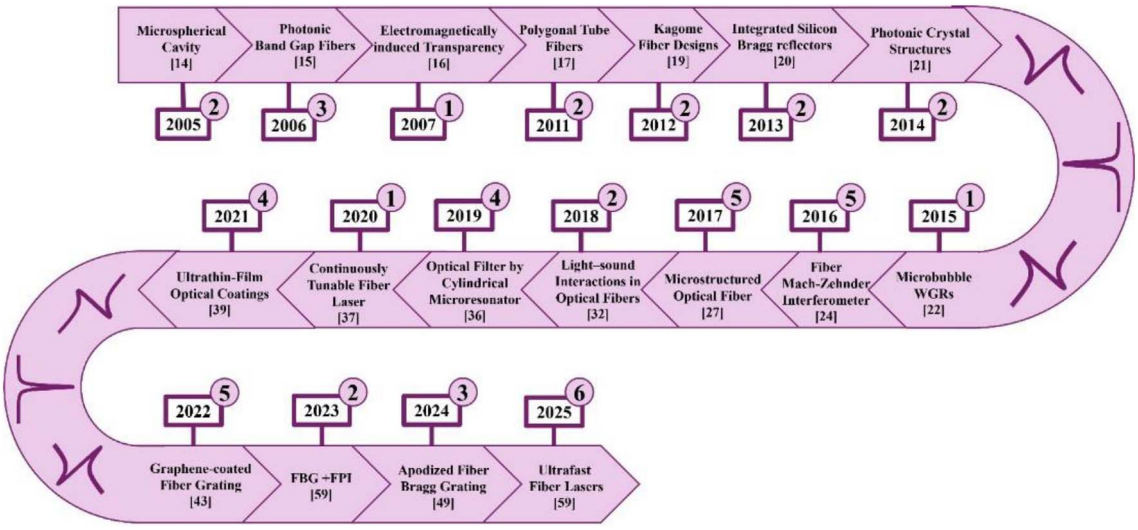

Fig. 2. The timeline on Fano resonance in fiber-optic structures illustrates a significant increase in the annual number of articles published between 2005 and 2025.

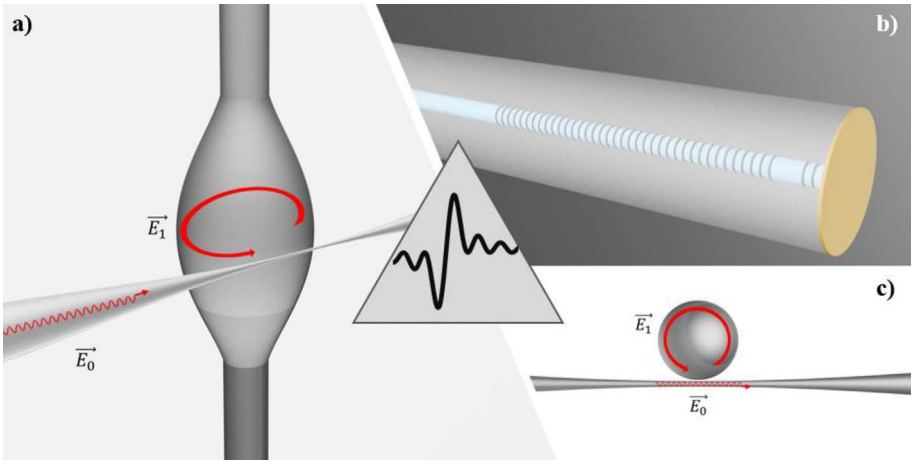

Fig. 3. Optical fiber structures that enable a Fano-like spectrum: a) a microbubble coupled to a taper fiber [22], b) a Bragg grating etalon-based optical fiber [52], c) a microsphere coupled to a taper fiber as a whispering-gallery resonators [14].

enhanced Fano resonance in a non-adiabatic tapered fiber coupled with a microresonator, demonstrating its potential for high-sensitivity optical sensing and laser stabilization.

In 2018, Pant et al. [32] reported wideband excitation of Fano resonances and induced transparency through coherent interactions between multiple Brillouin resonances, revealing a new mechanism for controlling light–sound interactions in optical fibers. In the same year, Zhang et al. [33] proposed an in-line fiber Michelson interferometer designed to enhance the Q-factor of cone-shaped in-wall capillary–coupled resonators, providing improved mode confinement and sharper resonance features.

In 2019, Jiang et al. [34] demonstrated Fano-like resonance in an all-fiber structure, achieving high spectral asymmetry and tunability through precise control of fiber coupling conditions. Lu et al. [35] reported tunable oscillating Fano spectra in a fiber taper–coupled conical microresonator, showing dynamic control of resonance profiles by adjusting the coupling gap and taper diameter. Wang et al. [36] proposed an ultranarrow optical filter based on Fano resonance in a single cylindrical microresonator, enabling single-longitudinal-mode operation in fiber lasers with high spectral purity. Tsai et al. [37] simulated a numerically method to minimize Fresnel reflections with an inscribed FBG at the fiber tip.

In 2020, Li et al. [38] introduced a continuously tunable fiber laser based on a Fano resonance filter using a thin fiber taper–coupled conical microresonator. This configuration allowed stable single-mode lasing and continuous wavelength tuning, demonstrating the potential of Fano-resonant devices for narrow-linewidth laser design and precision optical sensing.

In 2021, Li et al. [39] realized and modulated Fano-like lineshapes in fiber Bragg gratings, providing new insight

into dynamic control of asymmetric spectral responses via refractive index (RI) modulation. ElKabbash et al. [40] investigated Fano-resonant ultrathin-film optical coatings, enabling enhanced light–matter interactions and tunable spectral asymmetry in nanoscale photonic structures. Hu et al. [41] reported a laser-controlled Fano resonance sensing mechanism based on WGM coupling in eccentric-hole fibers integrated with azobenzene materials, achieving optically tunable sensitivity through photochemical modulation. Li et al. [42] developed a fiber Fabry–Perot interferometer-based Fano resonance coupler for whispering-gallery-mode resonators, improving coupling efficiency and enhancing the Q-factor through hybrid cavity interactions.

In 2022, Sun et al. [43] proposed a quasi-3D Fano resonance cavity integrated on the end-facet of an optical fiber for high signal-to-noise ratio "dip-and-read" surface plasmon sensing. This configuration provides a compact and robust sensing platform capable of real-time refractive index monitoring, ideal for biosensing and chemical detection with excellent signal fidelity. Jiang et al. [44] introduced an electrically tunable Fano-like resonance in a graphene-coated fiber grating, enabling fast, reversible modulation through electrical biasing – a step toward reconfigurable photonic systems for sensing and communication. Zhu and Yin [45] investigated Fano-resonance-based optical fiber characteristics for blood glucose detection, leveraging sharp asymmetric spectral features for high RI sensitivity in biomedical sensing. Aman et al. [46] combined the Vernier effect with Fano resonance to realize an ultra-sensitive all-optical sensor, where the Vernier amplification and Fano asymmetry jointly enhanced detection precision. Kudashkin et al. [47] developed a self-stabilized whispering gallery mode resonator in active-core fibers using negative feedback to maintain spectral stability under environmental fluctuations.

In 2023, Gan et al. [48] reported a Fano-like spectrum with quasi-independent slope ratio tuning by coupling higher-order HE modes with WGMs, enabling fine control of spectral asymmetry and linewidth. Finally, Sakhabutdinov et al. [49] proposed a hybrid FBG–FP structure producing composite Fano-type resonances with sharp, tunable spectra, suitable for precision strain, temperature, and pressure measurements.

In 2024, Wang et al. [50] reported an all-optical modulation of Fano-like resonances in an apodized fiber Bragg grating using Er/Yb-doped fiber. The nonlinear gain dynamics of the doped medium enabled effective modulation of the Fano profile without external electronics, demonstrating a new route toward all-optical control and tunable photonic filtering. Chai et al. [51] investigated Fano resonance in a microcylinder–taper coupling system for liquid RI sensing based on the axial separation method. By precisely adjusting the taper–cavity distance, the system achieved strong interference between localized and continuum modes, allowing high-resolution detection of RI variations in liquids. La et al. [52] demonstrated a Bragg etalon-based optical fiber for optoacoustic detection. Robalinho et al. [53] introduced a phase-shifted FBG (PS-FBG), which was fabricated using selective pitch slicing. This enabled tuning of the Fano-like asymmetry spectrum, resulting in a wide-range vibrational sensor. Feng et al. [54] proposed a simple scheme to generate multiple ultra-high-slope Fano-like resonances via Mach–Zehnder interferometers (MZIs) cascaded with fiber gratings. The configuration achieved enhanced spectral discrimination and steep transmission slopes, suitable for high-resolution spectral sensing and wavelength filtering.

In 2025, Wu et al. [55] presented a method for the synchronous and controllable realization of Lorentzian, Fano, and electromagnetically induced transparency (EIT) lineshapes in an all-fiber configuration. This work demonstrated full optical tunability between distinct resonance profiles within a single platform, significantly expanding the flexibility of all-fiber photonic filters and sensors. Li et al. [56] explored Fano resonance in a whispering gallery mode microsphere resonator coupled with a femtosecond laser-drilled tapered fiber. The laser-drilled taper provided enhanced coupling precision and mechanical stability, resulting in sharper resonance lines and improved sensing repeatability. Wang et al. [57] developed a modulation-free laser frequency stabilization technique based on balanced detection of a common-path Fano resonance in an all–polarization-maintaining (PM) fiber cavity. This approach provided a compact and vibration-insensitive means of laser locking, eliminating the need for active modulation or complex feedback electronics. Li et al. [58] proposed a mechanism to enhance the dynamic range in microcavity sensing through nonlinear harmonic generation of Fano resonances. The introduction of higher-order nonlinear interactions broadened the measurable range while preserving spectral sensitivity, enabling versatile performance in high-intensity or nonlinear photonic environments. Finally, Zou et al. [59] investigated the resonantly driven nonlinear dynamics of soliton molecules in ultrafast fiber lasers. The study revealed that soliton molecule formation and evolution could be strongly influenced by Fano-like interference effects within the laser cavity, providing new insights into the control of ultrafast nonlinear dynamics and pulse shaping in fiber lasers. Figure 3 summarizes the principal fiber-optic configurations employed with this technique.

4 Fano resonance on fiber structures

As outlined in the historical overview, various structures were designed to induce Fano resonance through modal coupling within the fiber. This section will address these architectures and their operational principles. The three most common approaches are whispering gallery modes, microstructured fibers and interferometric systems. Recently, new configurations using FBG structures were published to excite the discrete mode.

4.1 Whispering gallery mode microcavities

Whispering gallery modes are waves capable of propagating around a concave surface and were first presented as acoustic waves in 1910 [60]. In 1961, an electromagnetic analog was also demonstrated [61]. The microcavities used for WGM present advantages such as a high Q-factor and a comparatively reduced mode volume [62]. When coupled

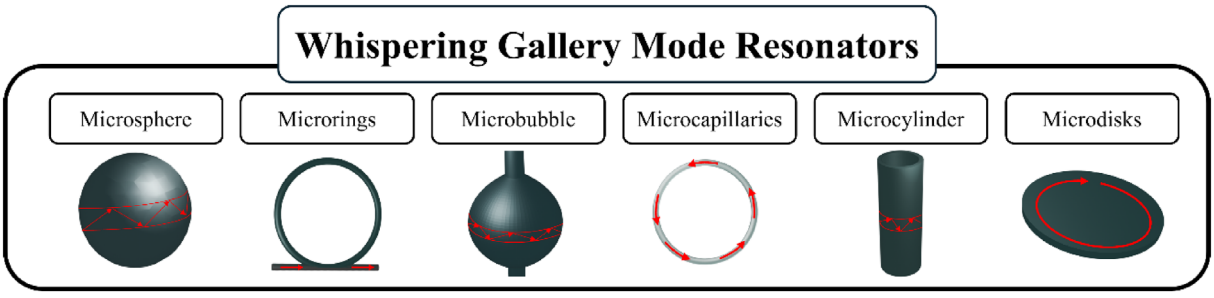

Fig. 4. Overview of WGM resonators used for induced Fano resonance coupled into optical fibers.

with an optical fiber, considered to have a low Q-factor and to propagate a continuum mode, the capacity to induce Fano resonance is enhanced due to its high Q-factor, which represents the discrete mode [63]. Two mathematical methodologies have been developed for modeling the modal interference between both. The classical transfer matrix method analyzes the exchange of optical power between the resonator and the waveguide [64]. The coupled mode theory, proposed by Pierce at Bell Laboratories, accounts for different fields that perturb the system to calculate the spectrum [65].

In literature, a wide range of structures have been developed to propose a WGM. These include microspheres [66], microrings [67], microbubble [68], microdisks [69], microcapillaries [70], microcylinder [71], microtoroid [72] and others. The coupled waveguide exhibits a low Q-factor and operates within a limited frequency range, thereby inducing the Fano phenomenon. The structure can be obtained through various methods, which can be classified into two distinct groups. Single-cavity coupling, defined as a coupling configuration in which only one cavity is involved, can be achieved through unilateral coupling, a process in which a resonator is coupled to the side of a single waveguide. For example, a WGM microcavity coupled to a tapered fiber [73] exhibits the advantages of simple fabrication, high coupling efficiency, and elevated Q-value in the order of 10^6 [74] and a maximum obtained of 10^8 [75]. However, it is considered a fragile system. Alternatively, bilateral coupling typically involves positioning the resonator between two waveguides [76]. Another approach is the in-fiber coupling structure, which enhances system robustness by embedding the resonator within the fiber waveguide [77, 78]. However, the Q-factor presents lower values compared to microresonators coupled to tapered fibers, being limited to 10^4 [33]. This demands further investigations of this method in order to fully exploit the potential of WGM resonators and the robustness of optical fibers. An overview of the resonator's structures mentioned is illustrated in Figure 4.

Another common approach is multi-cavity coupling, which comprises the same coupling types showed above: unilateral, bilateral, and in-fiber; however, it involves more than one microcavity interacting through resonance [79–83]. In comparison, multi-cavity coupling more readily excites resonances between a low-Q mode and a high-Q mode due to the resonant interactions among the microcavities coupled to the fiber. Figure 5 presents typical configurations of these resonators with an optical fiber, which can be unilateral, bilateral, or in-fiber.

4.2 Microstructured optical fibers

Microstructured optical fibers are structures that differ from the classic single-mode fiber, in which different structures are developed within the fiber to guide light along the direction of propagation. Typically, instead of a central core with a higher refractive index, air holes are introduced within the fiber. Geometry and spatial organization are determinant for the confined and propagated modes [84]. The Fano resonance is induced when the mode confinement geometry is designed to enable interaction between a high-Q mode and a low-Q mode.

An investigation was conducted on how the phase relationship between each hollow-core cylinder in a photonic bandgap fiber induces Fano-like resonances in the scattering spectrum [15]. In that study, the number of cylinders and their spacing were identified as critical parameters in coupling terms and Fano appearance. Another confinement mechanism is the Inhibited Coupling (IC), which provide a wider transmission bandwidth than PBG [85]. Distinct MOFs were designed to achieve IC, and this mechanism has been used to obtain Fano resonance in Kagome fibers [86] and polygonal tube fibers [17, 19].

4.3 Interferometric strutures

Interferometric structures have been widely used in photonics for a range of applications. In the context of Fano resonance, this phenomenon has been observed in a Mach-Zender interferometer (MZI), and a theorical model was developed by Miroshinichenko et al. [87]. Several applications have been demonstrated using such configurations, including sensing with a tapered optical fiber [88], an in-line MZI incorporating an FBG inscribed in a D-shaped fiber [34], and microrings exhibiting a discrete comb-like spectrum coupled to arm of an MZI [55]. MZI-based Fano resonances have also been explored for optical bistability [89], and for tunable control of the Fano asymmetry using FBGs [44, 50, 54, 90], demonstrating a versatile approach to inducing Fano resonance in all-fiber systems.

Michelson interferometer configurations have been demonstrated in an in-fiber integrated setup with a microsphere WGM for sensing and lasing applications [33], as well as in a ring-cavity-coupled scheme for optical bistabil-

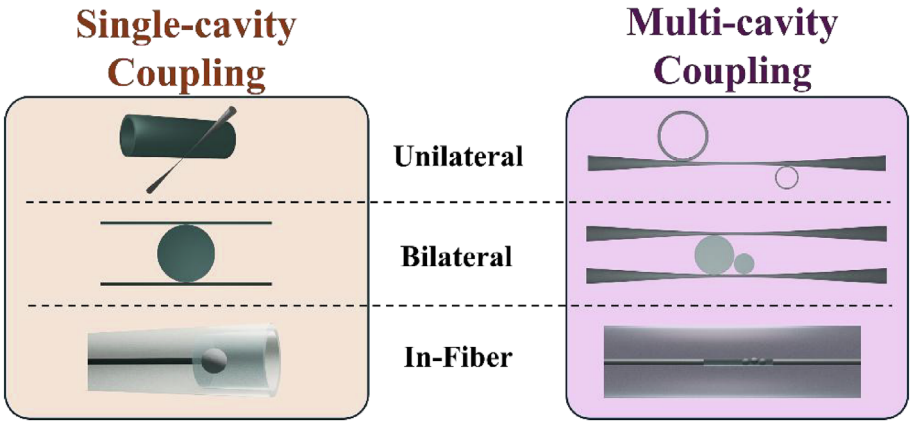

Fig. 5. Typical configurations of WGM resonators coupled to optical fibers to excite Fano resonance.

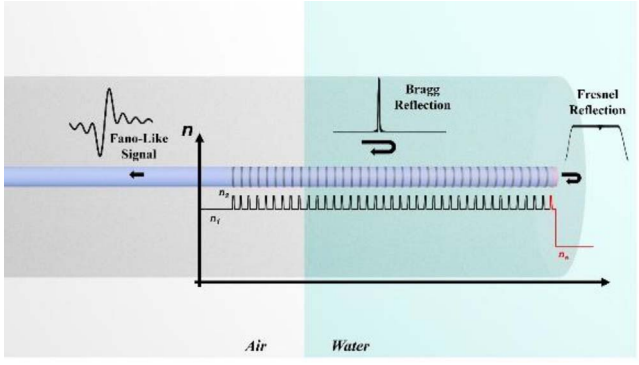

Fig. 6. Dynamic behavior of the Fano-FBG structure, where the interference between Fresnel and Bragg reflections results in the emergence of a Fano-like reflected spectrum.

ity [91]. Another approach relies on Fabry–Pérot interferometers (FPIs) coupled to a WGM microsphere [42], or combined with FBGs [49, 92, 93], where the interaction between the two elements induces a Fano-like resonance. FPI-based schemes have also been enhanced by integrating a gold plasmonic metasurface on the facet [94]. In contrast, Sagnac interferometers are less commonly used to induce Fano resonance in optical fibers, being more frequently reported in silicon waveguides [95].

4.4 Bragg gratings structures

This review briefly addresses one of the most recent works in optical fiber sensors, published in 2024, which proposes a Fano-like FBG structure, as illustrated in Figure 6 [53]. This FBG structure is a phase-shift grating operated in reflection, in which the last period is modified to introduce the phase shift; that is, its periodicity is shorter than the nominal FBG period. This study investigated a Fano-FBG configuration in which the reflectivity at the fiber end was kept fixed while the FBG reflectivity was varied. The inverse case was then analyzed: the FBG reflectivity was held constant, and the fiber-tip reflectivity was varied externally. The objective was to identify the optimal parameters for obtaining a well-defined Fano spectrum on an optical spectrum analyzer (OSA). Based on these simulations, the structure's performance as a refractive-index sensor was demonstrated both theoretically and experimentally, highlighting its advantages as a sensing element and showcasing the potential of this new configuration to the scientific community.

4.4.1 An analytical approach to modeling the Fano-like FBG

The interferometric phenomenon that yields the FBG spectrum can be described using coupled-mode theory, as presented by Sakhabutdinov et al. [49]. Another possibility is to study the interaction between the incident electric field amplitude E and the grating structure. In this approach, the model is based on summing the contributions of the waves reflected at each refractive-index perturbation introduced by the grating modulation. The grating period between the successive reflective points Λ introduces a phase shift of $\varphi = \beta(2\Lambda)$, where $\beta = 2\pi n_{\text{eff}}/\lambda_0$ the propagation coefficient, n_{eff} the effective refractive index, and λ_0 the vacuum wavelength. To model the superposition of reflections, N reflective points are defined to simulate the FBG, each characterized by transmission and reflection coefficients of $t_\Lambda = 2n_1n_2/n_1 + n_2$ and $r_\Lambda = (n_1 - n_2)/(n_1 + n_2)$, respectively, where n_1 is the optical fiber core refractive index and n_2 is the grating refractive index.

The Fano-like resonance arises from interference between a discrete spectrum and a continuum spectrum. In this framework, a spacing is introduced between the grating's last pitch and the fiber tip, with a length ranging from 0 and Λ. The continuum mode originates itself from the Fresnel reflection at the fiber tip across this final spacing,, with reflection coefficient of $R_\Phi = [(n_{\text{eff}} - n_e)/(n_{\text{eff}} + n_e)]^2$, where n_e is the environment RI. The phase shift is determined by this specific length Φ, which in turn controls the tuning of the Fano asymmetry parameter q. Equations (2) and (3) provide the mathematical model obtained by summing the reflected electromagnetic waves, that reproduces the Fano-like asymmetrical spectrum generated by the Fano-FBG. In this numerical model, the FBG response is expressed as a geometric series, with the

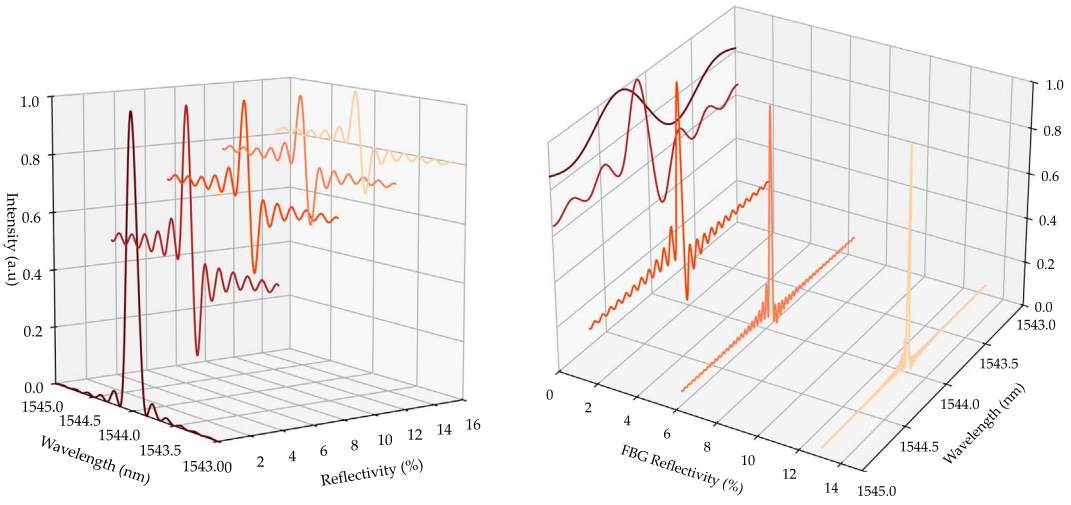

Fig. 7. Simulation of modal coupling efficiency: (a) influence of Fresnel reflectivity and (b) influence of the FBG reflected peak intensity on the resulting Fano profile.

Fresnel reflection at the fiber tip determined by the last term. The Fano parameter is controlled by the ratio between the length of the last pitch, Φ, and the Bragg period, Λ, of the FBG. For $\Phi \leq \Lambda/2$, the asymmetric line shapes correspond to Fano parameters between -1 and 0. When $\Phi = \Lambda/2$, the Fano parameter equals 0, whereas for $\Phi \geq \Lambda/2$, the Fano parameter lies between 0 and 1.

$$E_r = E\left[r_\Lambda \sum_{k=0}^{N} \left(t_\Lambda e^{i\beta\Lambda}\right)^{2k} + R_\Phi {t_\Lambda}^{2N+2} e^{i\beta(2\Phi+2N\Lambda)}\right], \quad (2)$$

$$E_r = E\left[\frac{\mathrm{r}_\Lambda\left(1-\left(t_\Lambda e^{i\beta\Lambda}\right)^{2N+2}\right)}{\left(1-\left(t_\Lambda e^{i\beta\Lambda}\right)^{2}\right)} + R_\Phi {t_\Lambda}^{2N+2} e^{i\beta(2\Phi+2N\Lambda)}\right]. \quad (3)$$

Based on the analytical model, the coupling efficiency of the Fano-FBG is investigated as a function of both the grating reflectivity and the Fresnel reflection coefficient at the fiber tip. In this analysis, the grating length is kept constant at 1 mm. In Figure 7a, the parameter R_Φ (0–3%) quantifies the strength of the secondary reflection that couples with the grating-reflected field. As R_Φ increases, the response evolves from a conventional, symmetric FBG spectrum (0%) to a clearly asymmetric Fano line shape (3%), evidencing progressively stronger interference. Figure 7b considers the Fresnel reflection associated with the silica–air interface at the fiber end, while the FBG reflectivity is swept from 0.1% to 13%. Increasing grating reflectivity reduces the relative contribution of the tip-reflected field, weakening the interference term; consequently, the grating-reflected component dominates and the Fano features progressively vanish. Conversely, higher tip reflectivity enhances the counter-propagating field, increasing the interference contrast and sharpening the Fano spectral asymmetry. Moreover, large grating reflectivity compresses the spectral bandwidth and drives the response toward the characteristic FBG peak, effectively masking the Fano profile. Therefore, achieving efficient modal coupling and inducing the Fano resonance requires a suitable trade-off between grating and tip reflectivities, ensuring comparable amplitudes of the two interfering reflected signals. Another relevant aspect is the tunability of the Fano asymmetric q - parameter via the phase shift introduced in the FBG. By adjusting the length of the final grating period, one can realize different interference regimes, yielding $q = \pm 1$ and $q = 0$. Notably, the case $q = 0$ corresponds to a symmetric FBG notch response or anti-reflection AR-FBG, as reported in [37]. For $q = \pm 1$, a representative example is provided by the 2024 study on the slice FBG approach [53], where this phase-shift produces a clearly asymmetric Fano profile.

4.4.2 Fano-like FBG applied as a sensing tool

In addition to the simulation work performed for the optical device, an experimental study was also carried out to evaluate its performance as a sensor for monitoring refractive-index variations in liquids. Different water–sugar solutions were prepared to obtain refractive indices ranging from 1.334 to 1.339. The experiments were performed using a Fano-like FBG with $q = -1$ (see Fig. 8a). The interrogation system was intensity-based, and self-referenced by measuring the intensity difference between the peak and the valley of the Fano profile; the experimental and numerical results are illustrated in Figure 8b. This approach was chosen because the Fresnel reflectivity strongly influences the signal intensity, while the peak wavelength exhibits low sensitivity to refractive-index variations. The experimental setup comprised broadband source with a spectral bandwidth of 100 nm centered at 1550 nm, a three-port optical fiber circulator (Thorlabs 6015-3) to route the reflected

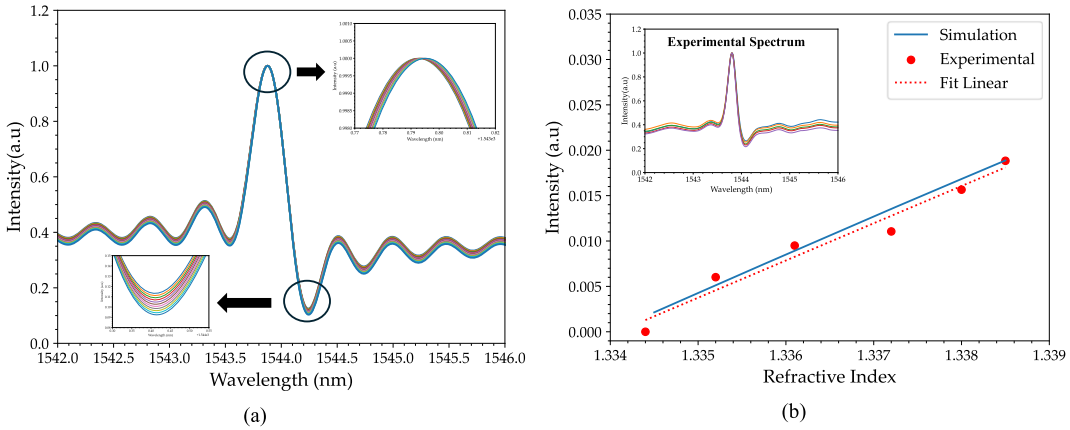

Fig. 8. Evaluation of the Fano-FBG, with $q = -1$, as an optical fiber sensor: a) simulated spectrum and b) comparison between the simulation predictions and the experimental results.

Table 1. RI sensors based on FBGs.

	Detection Limit (RIU)	Ref
FBG and etch-eroded fiber Fabry-Pérot interferometer	1.4×10^{-5}	[96]
Thinned fiber Bragg gratings	10^{-4}	[97]
Dual Fabry-Perot FBG	10^{-5}	[98]
End-face of a glass fiber connected to FBG	10^{-3}	[99]
In this Work (Fano-FBG)	6×10^{-4}	

signal, and an Optical Spectrum Analyzer (YOKOGAWA AQ6370C, Osaka, Japan) for spectral interrogation. The fiber-tip cleaving process was achieved using a polishing machine, with the support of the OSA, the fiber tip can be polished until the desire asymmetry is obtained (Table 1).

The validation of the mathematical model was performed by comparing the intensity variation within the defined refractive-index range. The simulations resulted in an FBG with 1% reflectivity, $\Delta n = 2.6 \times 10^{-4}$, and $N = 8452$. Experimentally, a linear sensitivity of 4.1 ± 0.4 RIU^{-1} was obtained ($r^2 = 0.980$), while the simulation yielded a linear sensitivity of 4.18 ± 0.01 RIU^{-1} ($r^2 = 0.99997$). The experimental results also indicated a detection limit of 6×10^{-4} RIU. A deviation of approximately 1% was observed between the real sensor performance and the simulation predictions, as demonstrated in Figure 8b. This demonstration shows the potential of a Fano-like FBG as a sensing element, both for wavelength-based measurements as temperature measurement and for self-referenced intensity measurements. In this case, it is possible to use two lasers with wavelengths set at each peak and apply filtering to separate the wavelength contributions. Thus, by using two photodetectors, we obtain a low-cost system. A comparison with other RI sensors reveals that this system provides measurement capabilities comparable to other intensity-based interrogation FBG systems. Also, it offers a simpler implementation for achieving higher sensitivity than many existing approaches, highlighting its potential as an effective optical sensing device.

5 Conclusion

The chronological evolution of studies on Fano resonance in optical fiber systems – from its early conceptual demonstrations in the mid-2000s to the highly integrated and tunable devices developed after 2020 – illustrates a clear trajectory toward functional maturity and application-oriented design. Early works focused on demonstrating the physical existence of Fano interference in guided-wave structures and microresonators, whereas more recent contributions have emphasized engineering control, spectral reconfigurability, and hybrid material integration. The demonstration of the Fano-like FBG highlights the potential of this structure as a simple device capable of exciting a Fano-like resonance. When demonstrated as a RI sensor with a resolution of 6×10^{-4} RIU, the sensitivity is not remarkable; however, the self-referencing method is useful for reducing the influence of external noise on the measurement. Looking to the future, research is expected to converge on several key directions. First, the integration of intelligent control mechanisms, such as thermo-optic, electro-optic, and opto-mechanical tuning, will likely enable adaptive Fano resonance devices capable of self-calibration and real-time environmental compensation. These developments may render Fano-based sensors and filters not only highly sensitive but also self-stabilizing and field-deployable for operation in harsh or dynamic environments. The ongoing miniaturization trend in photonic integration suggests that Fano-resonant fiber systems may evolve toward chip-scale architectures, maintaining the low-loss advantages of

optical fibers while achieving full compatibility with silicon photonics and planar integrated circuits. This evolution could lead to compact, mass-producible Fano-based devices directly integrated into telecommunication, biomedical, and quantum systems. In summary, the coming decade is poised to witness the emergence of adaptive, multifunctional, and miniaturized Fano-resonant fiber systems, bridging the gap between fundamental photonics and real-world applications.

Acknowledgments

This work is funded by national funds through FCT – Fundação para a Ciência e a Tecnologia, I.P., under the support UID/50014/2025 (https://doi.org/10.54499/UID/50014/2025. This work was also carried out under Project No. 15022 (ACLART – Prediction of clinical outcomes of anterior cruciate ligament reconstruction through in silico simulation combined with artificial intelligence), reference COMPETE2023-FEDER-00867200. The project was co-financed by the European Regional Development Fund (ERDF) under the PORTUGAL2030 program, and by the budget of the Foundation for Science and Technology, I.P. (FCT).

Conflicts of interest

The authors have nothing to disclose.

Data availability statement

This article has no associated data generated and/or analyzed / Data associated with this article cannot be disclosed due to legal/ethical/other reason.

Author contribution statement

We expect that all authors will have reviewed, discussed, and agreed to their individual contributions ahead of this time. Contributions will be published before the references section, and they should accurately reflect contributions to the work. The Conceptualization, O. Frazão and V. Piaia; Software, V. Piaia. and P. Robalinho; Validation, S. Silva and O. Frazão.; Writing – Original Draft Preparation, O. Frazão and V. Piaia; Writing – Review & Editing, P. Robalinho and S. Silva.; Supervision, O. Frazão.

References

1 Cao G, Dong S, Zhou L-M, Zhang Q, Deng Y, Wang C, Zhang H, Chen Y, Qiu C-W, Liu X, Fano resonance in artificial photonic molecules, *Adv. Opt. Mater.* **8**, 1902153 (2020). https://doi.org/10.1002/adom.201902153.

2 Rasmussen TS, Yu Y, Mork J, Theory of self-pulsing in photonic crystal Fano lasers, *Laser Photonics Rev.* **11**, 1700089 (2017). https://doi.org/10.1002/lpor.201700089.

3 Lim WX, Manjappa M, Pitchappa P, Singh R, Shaping high-Q planar Fano resonant metamaterials toward futuristic technologies, *Adv. Opt. Mater.* **6**, 1800502 (2018). https://doi.org/10.1002/adom.201800502.

4 Sulabh, Singh L, Jain S, Kumar M, Nanophotonic device based on Fano resonance in engineered slot waveguide for optical detection of viral infections, *IEEE Sens. J.* **21**, 2805–2812 (2021). https://doi.org/10.1109/JSEN.2020.3023146.

5 Bekele D, Yu Y, Yvind K, Mork J, In-plane photonic crystal devices using Fano resonances, *Laser Photonics Rev.* **13**, 1900054 (2019). https://doi.org/10.1002/lpor.201900054.

6 Abujetas DR, Mandujano MAG, Méndez ER, Sánchez-Gil JA, High-contrast Fano resonances in single semiconductor nanorods, *ACS Photonics* **4**, 1814–1821 (2017). https://doi.org/10.1021/acsphotonics.7b00395.

7 Chen J, Gan F, Wang Y, Li G, Plasmonic sensing and modulation based on Fano resonances, *Adv. Opt. Mater.* **6**, 1701152 (2018). https://doi.org/10.1002/adom.201701152.

8 Dong G, Wang Y, Zhang X (2018) High-contrast and low-power all-optical switch using Fano resonance based on a silicon nanobeam cavity, *Opt. Lett.* **43**, 5977–5980. https://doi.org/10.1364/OL.43.005977.

9 Yu Y, Hu H, Oxenløwe LK, Yvind K, Mork J, Ultrafast all-optical modulation using a photonic-crystal Fano structure with broken symmetry, *Opt. Lett.* **40**, 2357–2360 (2015). https://doi.org/10.1364/OL.40.002357.

10 Solodovchenko N, Sidorenko M, Seidov T, Popov I, Nenasheva E, Samusev K, Limonov M, Cascades of Fano resonances in light scattering by dielectric particles, *Mater. Today* **60**, 69–78 (2022). https://doi.org/10.1016/j.mattod.2022.09.007.

11 Zangeneh-Nejad F, Fleury R, Topological Fano resonances, *Phys. Rev. Lett.* **122**, 014301 (2019). https://doi.org/10.1103/PhysRevLett.122.014301.

12 Fano U, Effects of configuration interaction on intensities and phase shifts, *Phys. Rev.* **124**, 1866–1878 (1961). https://doi.org/10.1103/PhysRev.124.1866.

13 Limonov MF, Rybin MV, Poddubny AN, Kivshar YS, Fano resonances in photonics, *Nature Photon.* **11**, 543–554 (2017). https://doi.org/10.1038/nphoton.2017.142.

14 Chiba A, Fujiwara H, Hotta J, Takeuchi S, Sasaki K, Fano resonance in a multimode tapered fiber coupled with a microspherical cavity, *Appl. Phys. Lett.* **86**, 261106 (2005). https://doi.org/10.1063/1.1951049.

15 Steinvurzel P, de Sterke CM, Steel MJ, Kuhlmey BT, Eggleton BJ, Single scatterer Fano resonances in solid core photonic band gap fibers, *Opt. Express* **14**, 8797–8811 (2006). https://doi.org/10.1364/OE.14.008797.

16 Totsuka K, Kobayashi N, Tomita M, Slow light in coupled-resonator-induced transparency, *Phys. Rev. Lett.* **98**, 213904 (2007). https://doi.org/10.1103/PhysRevLett.98.213904.

17 Vincetti L, Setti V, Fano resonances in polygonal tube fibers, *J. Lightwave Technol.* **30**, 31–37 (2012). https://doi.org/10.1109/JLT.2011.2177245.

18 Li B-B, Xiao Y-F, Zou C-L, Liu Y-C, Jiang X-F, Chen Y-L, Li Y, Gong Q, Experimental observation of Fano resonance in a single whispering-gallery microresonator, *Appl. Phys. Lett.* **98**, 021116 (2011). https://doi.org/10.1063/1.3541884.

19 Vincetti L, Setti V, Extra loss due to Fano resonances in inhibited coupling fibers based on a lattice of tubes, *Opt. Express* **20**, 14350–14361 (2012). https://doi.org/10.1364/OE.20.014350.

20 Chang C-M, Solgaard O, Fano resonances in integrated silicon Bragg reflectors for sensing applications, *Opt. Express* **21**, 27209–27218 (2013). https://doi.org/10.1364/OE.21. 027209.

21 Yu Y, Heuck M, Hu H, Xue W, Peucheret C, Chen Y, Oxenløwe LK, Yvind K, Mørk J, Fano resonance control in a photonic crystal structure and its application to ultrafast switching, *Appl. Phys. Lett.* **105**, 061117 (2014). https://doi.org/10.1063/1.4893451.

22 Yang Y, Saurabh S, Ward J, Chormaic SN, Coupled-mode-induced transparency in aerostatically tuned microbubble whispering-gallery resonators, *Opt. Lett.* **40**, 1834–1837 (2015). https://doi.org/10.1364/OL.40.001834.

23 Miao Y, Peng Y, Xiang Y, Li M, Lu Y, Song Y, Dynamic Fano resonance in thin fiber taper coupled cylindrical microcavity, *IEEE Photonics J.* **8**, 1–6 (2016). https://doi.org/10.1109/JPHOT.2016.2630316.

24 Zhao C, Gan X, Fang L, Han L, Chang K, Li D, Zhao J, Tunable Fano-like resonance enabled by coupling a microsphere with a fiber Mach–Zehnder interferometer, *Appl. Opt.* **55**, 5756–5760 (2016). https://doi.org/10.1364/AO.55.005756.

25 Gu B, Zhou Y, Yu X, Luan F, Fiber loop laser stabilized by Fano resonance in metallic grating coupled resonator, *IEEE Photonics Technol. Lett.* **28**, 1597–1600 (2016). https://doi.org/10.1109/LPT.2016.2560239.

26 Liao J, Wu X, Liu L, Xu L, Fano resonance and improved sensing performance in a spectral-simplified optofluidic micro-bubble resonator by introducing selective modal losses, *Opt. Express* **24**, 8574–8580 (2016). https://doi.org/10.1364/OE.24.008574.

27 Lin W, Zhang H, Chen S-C, Liu B, Liu Y-G, Microstructured optical fiber for multichannel sensing based on Fano resonance of the whispering gallery modes, *Opt. Express* **25**, 994–1004 (2017). https://doi.org/10.1364/OE.25.000994.

28 Miao Y, Li M, Song Y (2017) Ring fiber lasers based on EIT-like Fano resonances as a wavelength-selective element, *IEEE Photonics Technol. Lett.* **29**, 1900–1902. https://doi.org/10.1109/LPT.2017.2755696.

29 Li S, Wang Y, Jiao R, Wang L, Duan G, Yu L, Fano resonances based on multimode and degenerate mode interference in plasmonic resonator system, *Opt. Express* **25**, 3525–3533. https://doi.org/10.1364/OE.25.003525.

30 Zhang X, Yang Y, Shao H, Bai H, Pang F, Xiao H, Wang T, Fano resonances in cone-shaped inwall capillary based microsphere resonator, *Opt. Express* **25**, 615–621 (2017). https://doi.org/10.1364/OE.25.000615.

31 Zhang K, Wang Y, Wu Y-H, Enhanced Fano resonance in a non-adiabatic tapered fiber coupled with a microresonator, *Opt. Lett.* **42**, 2956–2959 (2017). https://doi.org/10.1364/OL.42.002956.

32 Pant R, Siva Shakthi A, Yelikar AB, Wideband excitation of Fano resonances and induced transparency by coherent interactions between Brillouin resonances, *Sci. Rep.* **8**, 9175 (2018). https://doi.org/10.1038/s41598-018-27444-8.

33 Zhang X, Bai H, Pan H, Wang J, Yan M, Xiao H, Wang T, In-line fiber michelson interferometer for enhancing the Q factor of cone-shaped inwall capillary coupled resonators, *IEEE Photonics J.* **10**, 1–8 (2018). https://doi.org/10.1109/JPHOT.2018.2818715.

34 Jiang B, Gan X, Gu L, Hao Z, Wang S, Bi Z, Zhang L, Zhou K, Zhao J, Fano-like resonance in an all-in-fiber structure, *IEEE Photonics J.* **11**, 1–7 (2019). https://doi.org/10.1109/JPHOT.2019.2936485.

35 Lu Y, Zhu X, Li J, Nie Y, Li M, Song Y, Tunable oscillating Fano spectra in a fiber taper coupled conical microresonator, *IEEE Photonics J.* **11**, 1–7 (2019). https://doi.org/10.1109/JPHOT.2019.2924257.

36 Wang H, Xu R, Zhang J, Zhou W, Shen D, Ultranarrow filter based on Fano resonance in a single cylindrical microresonator for single-longitudinal-mode fiber lasers, *Opt. Express* **27**, 22717–22726 (2019). https://doi.org/10.1364/OE.27.022717.

37 Tsai T-Y, Lee Z-C, Tsao H-X, Lin S-T, Minimization of Fresnel reflection by anti-reflection fiber Bragg grating inscribed at the fiber ends, *Opt. Express* **27**, 11510–11515 (2019). https://doi.org/10.1364/OE.27.011510.

38 Li J, Lu Y, Cao L, Li M, Song Y, Continuously tunable fiber laser based on Fano resonance filter of thin-fiber-taper-coupled conical microresonator, *Opt. Commun.* **466**, 125629 (2020). https://doi.org/10.1016/j.optcom.2020.125629.

39 Li A, Jiang B, Zhang P, Gan X, Hao Z, Hou Y, Zhang J, Li P, Zhao J, Realization and modulation of Fano-like lineshape in fiber Bragg gratings, *J. Lightwave Technol.* **39**, 4419–4423 (2021). https://opg.optica.org/jlt/abstract.cfm?uri=jlt-39-13-4419.

40 ElKabbash M, Letsou T, Jalil SA, Hoffman N, Zhang J, Rutledge J, Lininger AR, Fann C-H, Hinczewski M, Strangi G, Guo C, Fano-resonant ultrathin film optical coatings, *Nat. Nanotechnol.* **16**, 440–446 (2021). https://doi.org/10.1038/s41565-020-00841-9.

41 Hu X, Zhang H, Lin W, Wang Y, Liu B, Laser-controlled Fano resonance sensing based on WGM coupling in eccentric hole fibers integrated with azobenzene, *J. Lightwave Technol.* **39**, 320–327 (2021). https://opg.optica.org/jlt/abstract.cfm?uri=jlt-39-1-320.

42 Li M, Wang R, Fiber Fabry-Perot interferometer-based Fano resonance coupler for whispering-gallery-mode resonators, *IEEE Photonics Technol. Lett.* **33**, 585–588(2021). https://doi.org/10.1109/LPT.2021.3076999.

43 Sun X, Lei Z, Zhong H, He C, Liu S, Meng Q, Liu Q, Chen S, Kong X, Yang T, A quasi-3D Fano resonance cavity on optical fiber end-facet for high signal-to-noise ratio dip-and-read surface plasmon sensing, *Light Adv. Manuf.* **3**, 665–675 (2022). https://doi.org/10.37188/lam.2022.046.

44 Jiang B, Zhang X, Li A, Hou Y, Hao Z, Gan X, Zhao J, Electrically induced dynamic Fano-like resonance in a graphene-coated fiber grating, *Photon. Res.* **10**, 1238–1243 (2022). https://doi.org/10.1364/PRJ.453762.

45 Zhu J, Yin J, Optical-fibre characteristics based on Fano resonances and sensor application in blood glucose detection, *Opt. Express* **30**, 26749–26760 (2022). https://doi.org/10.1364/OE.463427.

46 Hairol Aman MA, Ahmad Noorden AF, Ahmad Fajri FA, Abdul Kadir MZ, Bahari I, Danial WH, Daud S, Bahadoran M, Integrating Vernier spectrum with Fano resonance for high sensitivity of an all-optical sensor, *J. Comput. Electron.* **22**, 276–287 (2023). https://doi.org/10.1007/s10825-022-01946-1.

47 Kudashkin DV, Khorev SV, Vatnik ID. Self-Stabilization by negative feedback of whispering gallery mode resonators based on optical fiber with active core. *J. Lightwave Technol.* **40**, 7351–7357 (2022). https://doi.org/10.1109/JLT.2022.3201655.

48 Gan X, Ban Z, Gao F, Bo F, Zhang G, Xu J, Fano-like spectrum with a quasi-independent tuning of slope ratio based on HE mode components coupled whispering gallery mode, *J. Lightwave Technol.* **41**, 2501–2505 (2023). https://doi.org/10.1109/JLT.2022.3231243.

49 Sakhabutdinov AZh, Agliullin TA, Hussein SMRH, Kuznetsov AA, Anfinogentov VI, Valeev BI, Fano-type resonance structures based on combination of fiber Bragg grating with Fabry-Perot interferometer, *Karbala International Journal of Modern Science* **9** (2023). https://doi.org/10.33640/2405-609X.3279.

50 Wang F, Lin S, Qu Y, Han X, Wei Y, Zhao Z, Zhang Y, All-optical modulation of Fano-like resonances in apodized fiber Bragg grating using Er/Yb doped fiber, *J. Phys. D: Appl.*

Phys. **57**, 135104 (2024). https://doi.org/10.1088/1361-6463/ad194e.
51 Chai M, Liu C, Wang M, Xue C, Xie C, Xu W, Shi J, Wu T, He X, Fano resonance in a microcylinder-taper coupling system for liquid refractive index sensing via axial separation method, *Opt. Lasers Eng.* **179**, 108253 (2024). https://doi.org/10.1016/j.optlaseng.2024.108253.
52 La TA, Ülgen O, Shnaiderman R, Ntziachristos V, Bragg grating etalon-based optical fiber for ultrasound and optoacoustic detection, *Nat. Commun.* **15**, 7521 (2024). https://doi.org/10.1038/s41467-024-51497-1.
53 Robalinho P, Piaia V, Soares L, Novais S, Ribeiro AL, Silva S, Frazão O, Phase-shifted fiber Bragg grating by selective pitch slicing, *Sensors* **24**, 6898 (2024). https://doi.org/10.3390/s24216898.
54 Feng D, Zhang P, Yang Q, Wu J, Zhao J, Jiang B, Generation of multiple and ultra-high slope Fano-like resonances via MZI and cascaded fiber gratings, *Opt. Lasers Eng.* **194**, 109223 (2025). https://doi.org/10.1016/j.optlaseng.2025.109223.
55 Wu J, Xuan X, Liu Z, Zhang X, Li Y, Gan X, Jiang B, Synchronous and controllable realization of Lorentzian, Fano, and Electromagnetically induced transparency lineshapes in an all-fiber system, *J. Lightwave Technol.* **43**, 4435–4441 (2025). https://doi.org/10.1109/JLT.2025.3532642.
56 Li Z, Cai L, Liu Y, Jing H, Sun H, Xia F, Zhao Y, Fano resonance in a whispering gallery mode microsphere resonator coupled with femtosecond laser-drilled tapered fiber, *Opt. Laser Technol.* **187**, 112809 (2025). https://doi.org/10.1016/j.optlastec.2025.112809.
57 Wang J, Li Y, Chen Y, He S, Liu Q, Modulation-free laser frequency stabilization via balanced detection of common-path Fano resonance in all-PM fiber cavity, *APL Photonics* **10**, 076106 (2025). https://doi.org/10.1063/5.0275633.
58 Li J, Rong J, Xing E, Jia T, Xing T, Xing G, Yue H, Yang X, Zhou Y, Liu W, Tang J, Liu J, Enhancing dynamic range in microcavity sensing via nonlinear harmonic of Fano resonance, *J. Lightwave Technol.* **43**, 3792–3800 (2025). https://doi.org/10.1109/JLT.2025.3528044.
59 Zou D, Liu R, Shi Y, Zhang A, Li J, Chen GJ, Dang H, Song Y, Hu M, Shum PP, Resonantly driven nonlinear dynamics of soliton molecules in ultrafast fiber lasers, *Adv. Photonics* **7**, 016005 (2025). https://doi.org/10.1117/1.AP.7.1.016005.
60 Rayleigh L, CXII. The problem of the whispering gallery, *Philosophical Mag. Ser. 1* **20**, 1001–1004 (1910). https://www.tandfonline.com/doi/pdf/10.1080/14786441008636993.
61 Garrett CGB, Kaiser W, Bond WL, Stimulated emission into optical whispering modes of spheres, *Phys. Rev.* **124**, 1807–1809 (1961). https://doi.org/10.1103/PhysRev.124.1807.
62 Yu H, Liu X, Sun W, Xu Y, Liu X, Liu Y, A brief review of Whispering Gallery Mode in sensing, *Opt. Laser Technol.* **177**, 111099 (2024). https://doi.org/10.1016/j.optlastec. 2024.111099.
63 Cai L, Li S, Xiang F, Liu J, Liu Q, Fano resonance in whispering gallery mode microcavities and its sensing applications, *Opt. Laser Technol.* **167**, 109679 (2023). https://doi.org/10.1016/j.optlastec.2023.109679.
64 Yariv A, Universal relations for coupling of optical power between microresonators and dielectric waveguides, *Electron. Lett.* **36**, 321–322 (2000). https://doi.org/10.1049/el:20000340.
65 Huang W-P, Coupled-mode theory for optical waveguides: an overview, *J. Opt. Soc. Am. A* **11**, 963–983 (1994). https://doi.org/10.1364/JOSAA.11.000963.
66 Li S, Cai L, Li Z, Liu Y, Liu Q, Fano-like line shape and its tuning effect in a double-handle whispering gallery mode microsphere resonator, *J. Lightwave Technol.* **42**, 6881–6890 (2024). https://doi.org/10.1109/JLT.2024.3412099.
67 Chenari Z, Latifi H, Ranjbar-Naeini OR, Zibaii MI, Behroodi E, Asadollahi A, Tunable Fano-like lineshape in an adiabatic tapered fiber coupled to a hollow bottle microresonator, *J. Lightwave Technol.* **36**, 735–741 (2018). https://doi.org/10.1109/JLT.2017.2772260.
68 Liu W, Wang R, Li W, Zhang B, Xing E, Zhou Y, Sun P, Chen J, Tang J, Liu J, Modulation of Fano-like resonance in spherical microbubble cavity for high sensitivity pressure sensing, *Appl. Phys. Express* **15**, 046504 (2022). https://doi.org/10.35848/1882-0786/ac5c94.
69 Ji P, Zhu M, Liao C, Zhao C, Yang K, Xiong C, Han J, Li C, Zhang L, Liu Y, Wang Y, In-fiber polymer microdisk resonator and its sensing applications of temperature and humidity, *ACS Appl. Mater. Interfaces* **13**, 48119–48126 (2021). https://doi.org/10.1021/acsami.1c14499.
70 Guo Y, Zhang Y, Jiang W, Wu Y, Lineshape modulation and sensing characteristics of resonator assembled with liquid-metal core edge-coupled with microfiber coupler, *J. Lightwave Technol.* **40**, 2516–2522 (2022). https://doi.org/10.1109/JLT.2022.3142011.
71 Jin X, Dong Y, Wang K, Stable controlling of electromagnetically induced transparency-like in a single quasi-cylindrical microresonator, *Opt. Express* **24**, 29773–29780 (2016). https://doi.org/10.1364/OE.24.029773.
72 Xiao Y-F, Jiang X-F, Yang Q-F, Wang L, Shi K, Li Y, Gong Q, Tunneling-induced transparency in a chaotic microcavity, *Laser Photonics Rev.* **7**, L51–L54 (2013).
73 Zhang S, Li J, Yu R, Wang W, Wu Y, Optical multistability and Fano line-shape control via mode coupling in whispering-gallery-mode microresonator optomechanics, *Sci. Rep.* **7**, 39781 (2017). https://doi.org/10.1038/srep39781.
74 Veluthandath AV, Bhattacharya S, Murugan GS, Bisht PB, Fano resonances and photoluminescence in self-assembled high-quality-factor microbottle resonators, *IEEE Photonics Technol. Lett.* **31**, 226–229 (2019). https://doi.org/10.1109/LPT.2018.2889433.
75 Meng-Yu W, Ling-Jun M, Yu Y, Hui-Kai Z, Tao W, Bin L, Lei Z, Yan-Jun F, Ke-Yi W, Selection of whispering-gallery modes and Fano resonance of prolate microbottle resonators, *Acta Phys. Sin.* **69**, 234203–234210 (2020). https://doi.org/10.7498/aps.69.20200817.
76 Wang Y, Zhao H, Li Y, Shu F, Chi M, Xu Y, Wu Y, Mode splitting revealed by Fano interference, *Photon. Res.* **7**, 647–651 (2019). https://doi.org/10.1364/PRJ.7.000647.
77 Wang J, Zhang X, Yan M, Yang L, Hou F, Sun W, Zhang X, Yuan L, Xiao H, Wang T, Embedded whispering-gallery mode microsphere resonator in a tapered hollow annular core fiber, *Photon. Res.* **6**, 1124–1129 (2018). https://doi.org/10.1364/PRJ.6.001124.
78 Bai XQ, Wang DN, An in-fiber coupler for whispering-gallery-mode excitation in a microsphere resonator, *IEEE Photonics Technol. Lett.* **32**, 188–191 (2020). https://doi.org/10.1109/LPT.2020.2965972.
79 Yang G, Cai L, Liu J, Zhao Y, Zhang Z, Xiang F, Zhao Y, In-fiber three-cavity coupling of whispering gallery mode resonators for narrow Fano resonance, *Opt. Laser Technol.* **188**, 112966 (2025). https://doi.org/10.1016/j.optlastec. 2025.112966.
80 Li B-B, Xiao Y-F, Zou C-L, Jiang X-F, Liu Y-C, Sun F-W, Li Y, Gong Q, Experimental controlling of Fano resonance in indirectly

coupled whispering-gallery microresonators, *Appl. Phys. Lett.* **100**, 021108 (2012). https://doi.org/10.1063/1.3675571.
81 Li J, Qu Y, Wu Y, Add-drop double bus microresonator array local oscillators for sharp multiple Fano resonance engineering, *J. Appl. Phys.* **123**, 104305 (2018). https://doi.org/10.1063/1.5022091.
82 Ding M, Qin H, Yin Y, Transmission characteristics and Fano-like lineshape in coupled-slotted microresonators, *J. Lightwave Technol.* **38**, 3687–3693 (2020). https://doi.org/10.1109/JLT.2020.2980845.
83 Yang Y, Wang Z, Zhang X, Zhang Q, Wang T, Recent progress of in-fiber WGM microsphere resonator, *Front. Optoelectron.* **16**, 10 (2023). https://doi.org/10.1007/s12200-023-00066-3.
84 Eggleton BJ, Kerbage C, Westbrook PS, Windeler RS, Hale A, Microstructured optical fiber devices, *Opt. Express* **9**, 698–713 (2001). https://doi.org/10.1364/OE.9.000698.
85 Couny F, Benabid F, Roberts PJ, Light PS, Raymer MG, Generation and photonic guidance of multi-octave optical-frequency combs, *Science* **318**, 1118–1121 (2007). https://doi.org/10.1126/science.1149091.
86 Amsanpally A, Debord B, Alharbi M, Ilinova E, Vincetti L, Gérôme F, Benabid F, *Fano resonance in inhibited coupling Kagome fiber* (CLEO, 2015). Paper STu4L.6 STu4L.6. https://doi.org/10.1364/CLEO_SI.2015.STu4L.6.
87 Miroshnichenko AE, Kivshar YS, Mach–Zehnder–Fano interferometer, *Appl. Phys. Lett.* **95**, 121109 (2009). https://doi.org/10.1063/1.3232224.
88 Ahsani V, Ahmed F, Jun MBG, Bradley C, Tapered fiber-optic Mach-Zehnder interferometer for ultra-high sensitivity measurement of refractive index, *Sensors* **19**, 1652 (2019). https://doi.org/10.3390/s19071652.
89 Lu Y, Yao J, Li X, Wang P, Tunable asymmetrical Fano resonance and bistability in a microcavity-resonator-coupled Mach–Zehnder interferometer, *Opt. Lett.* **30**, 3069–3071 (2005). https://doi.org/10.1364/OL.30.003069.
90 Li A, Jiang B, Zhang P, Gan X, Hao Z, Hou Y, Zhang J, Li P, Zhao J, Realization and modulation of Fano-like lineshape in fiber Bragg gratings, *J. Lightwave Technol.* **39**, 4419–4423 (2021). https://opg.optica.org/jlt/abstract.cfm?uri=jlt-39-13-4419.
91 Li L, Zhang X, Chen L, Optical bistability and Fano-like resonance transmission in a ring cavity-coupled Michelson interferometer, *J. Opt. A: Pure Appl. Opt.* **10**:075305 (2008). https://doi.org/10.1088/1464-4258/10/7/075305.
92 Agliullin TA, Sakhabutdinov AZ, Valeev BI, Kazakov NA, Zakamskiy VK, Combination of fiber optical interferometric structures as a universal approach to sensor development, *Opt. Technol. Telecommun.* **13738**, 58–64 (2025). https://doi.org/10.1117/12.3067423.
93 Piaia V, Alves MR, Robalinho P, Silva S, Frazão O, Fano resonance of fiber Bragg grating for liquid sensing, *J. Lightwave Technol.* 1–7 (2025). https://doi.org/10.1109/JLT.2025.3642982.
94 Zhang L, Shang X, Cao S, Jia Q, Wang J, Yan W, Qiu M, Optical steelyard: high-resolution and wide-range refractive index sensing by synergizing Fabry–Perot interferometer with metafibers, *PhotoniX* **5**, 24 (2024). https://doi.org/10.1186/s43074-024-00138-3.
95 Arianfard H, Weiss T, Yang Y, Bader J, Castelletto S, Peruzzo A, *Fano-like resonances in coupled Sagnac interferometers formed by a self-coupled waveguide* (2025). https://doi.org/10.48550/arXiv.2511.07048.
96 Liang W, Huang Y, Xu Y, Lee RK, Yariv A, Highly sensitive fiber Bragg grating refractive index sensors, *Appl. Phys. Lett.* **86**, 151122 (2005). https://doi.org/10.1063/1.1904716.
97 Iadicicco A, Cusano A, Campopiano S, Cutolo A, Giordano M, Thinned fiber Bragg gratings as refractive index sensors, *IEEE Sens. J.* **5**, 1288–1295 (2005). https://doi.org/10.1109/JSEN.2005.859288.
98 Liu Y, Liu X, Ma C, Zhou Y, Micro-structured optical fiber sensor for simultaneous measurement of temperature and refractive index, *Opt. Fiber Technol.* **41**, 168–172 (2018). https://doi.org/10.1016/j.yofte.2018.01.019.
99 Sohn KR, Liquid sensors using refractive intensity at the end-face of a glass fiber connected to fiber-Bragg grating, *Sens. Actuators A Phys.* **158**, 193–197 (2010). https://doi.org/10.1016/j.sna.2009.12.039.